Journal of Chemical Health Risks

www.jchr.org

JCHR (2025) 15(6), 2101-2116 | ISSN:2251-6727

A Molecular Docking Approach for a Polymer-Based Nanofiber System for Wound Healing Applications

Ritu Hans[1] and Soumita Talukdar*

[1]Research Scholar, Center for Chemical & Biological Sciences, Process, Engineering and Technology, School of Engineering & Sciences, GD Goenka University, Gurgaon, India

(Received: 27 October 2025 Revised: 05 November 2025 Accepted: 04 December 2025)

KEYWORDS

Wound healing, molecular docking, polymeric nanofibers, PVA, Pectin, Na-CMC, polyamines, S1P.

ABSTRACT:

Introduction: Wound healing is a dynamic biological process responsible for repairing tissue damage and maintaining physiological balance. Modern wound dressings increasingly focus on multifunctional nanofibrous systems that are capable of delivering therapeutic strategies for accelerating tissue regeneration. Incorporating bioactive molecules such as small metabolites, lipid mediators, and amino acids into these polymeric nanofibers has emerged as a promising strategy to enhance angiogenesis, cell proliferation, and matrix remodeling key determinants of efficient wound regeneration.

Objective: The present study aims to evaluate, through in silico molecular docking, the potential of various small metabolites, lipid mediators, and amino acid derivatives incorporated into polymeric nanofibers composed of polyvinyl alcohol (PVA), pectin, and sodium carboxymethyl cellulose (Na-CMC), crosslinked with fumaric acid.

Methods: Polymeric nanofibers prepared using distilled water were treated as binding "targets" for molecular docking. Selected ligands included small metabolites (lactic acid, uric acid, polyamines—putrescine, spermidine, spermine) Lipid mediators (PGE2, PGF2α, LTB4, LTC4, LPC, S1P) Amino acids/metabolites (arginine, glutamine, glycine). Docking simulations were performed using AutoDock Vina and AGFR to evaluate ligand–nanofiber interactions.

Results: Docking analysis indicated that polyamines and sphingosine-1-phosphate (S1P) demonstrated the most favorable binding affinities with the nanocomposite. Their strong interactions suggest enhanced potential for influencing angiogenesis, fibroblast proliferation, and matrix remodeling when delivered via nanofibers.

Conclusion: These computational findings provide a theoretical foundation for developing multifunctional nanofiber wound dressings that combine structural support with biochemical signaling and antimicrobial capabilities, facilitating more effective wound repair.

1. Introduction:

Wound healing is a complex cascade of cellular, molecular and extracellular matrix events that proceed through ordered phases: hemostasis, inflammation, proliferation (granulation, angiogenesis, re-epithelization), and remodeling [1, 2]. Key challenges in chronic wounds, burns, or infected lesions are prolonged inflammation, impaired angiogenesis, microbial colonization, and aberrant matrix deposition [3]. This motivates the development of advanced wound dressings capable of providing structural support, promoting cell migration, and delivering bioactive molecules, while also controlling infection. Electrospun nanofibers have attracted considerable attention in wound-care applications because they mimic the architecture of the extracellular matrix (ECM), provide high surface area and porosity, and allow for incorporation of therapeutic agents [4-6]. For example, polymer blends of polyvinyl alcohol (PVA) and various natural polymers have been used to fabricate nanofiber wound dressings with favorable cell-adhesion and moisture-retention properties [7, 8]. In particular, PVA is a synthetic polymer widely used for biomedical scaffolds for its biocompatibility, hydrophilicity, and film-forming ability. Pectin and Na-CMC are natural polysaccharides

Journal of Chemical Health Risks

www.jchr.org

JCHR (2025) 15(6), 2101-2116 | ISSN:2251-6727

offering biodegradability, swelling capacity, and biocompatibility [9-11]. The combination of PVA/pectin/Na-CMC has been shown to improve mechanical, swelling, and moisture-management characteristics of wound dressing [12, 13]. Crosslinking with fumaric acid (a dicarboxylic acid) is used to stabilize the polymer network by esterification or ionic cross-links and reduce rapid dissolution in physiological fluids [14]. Beyond scaffold structure, the incorporation of nanoscale functional material can add further capabilities.

We explore the *in silico* docking of selected ligands representing wound-healing related small metabolites, lipid mediators, amino acid and other metabolites (lactic acid, uric acid, putrescine, spermidine, spermine, prostaglandins (PGE2/PGF2α), leukotrienes (LTB4/LTC4), lysophosphophatidylcholine, sphingosine-1-phosphate (S1P), arginine, glutamine, glycine) towards the nanofiber target systems. Each ligand contributes uniquely to wound-healing physiology. Lactic acid promotes angiogenesis and recruits endothelial progenitor cells, accelerating vascularization and repair [15]. Uric acid functions as an antioxidant and a damage-associated signal that modulates inflammation and recruits reparative cells [16]. Putrescine supports fibroblast proliferation and tissue regeneration, enhancing scaffold-mediated cell growth [17]. Spermidine accelerates re-epithelialization by promoting keratinocyte migration through uPA/uPAR pathway activation [18], while spermine aids keratinocyte proliferation and migration, facilitating epithelial closure [19]. Prostaglandins (PGE_2/$PGF_2\alpha$) regulate inflammation and angiogenesis, and their scaffold interaction may modulate healing dynamics [20]. Leukotrienes (LTB_4/LTC_4) influence leukocyte recruitment and vascular permeability, meaning their binding could regulate inflammation at the wound site [21]. Lysophosphatidylcholine (LPC) affects endothelial activation and inflammatory signaling, impacting local vascular responses [22]. Sphingosine-1-phosphate (S1P) promotes angiogenesis and keratinocyte migration, thus enhancing vascularized wound healing [23]. Arginine contributes to collagen synthesis and nitric oxide signaling, supporting fibroblast activity [24]. Glutamine provides nitrogen for proliferating immune and repair cells, sustaining the proliferative phase [25], while glycine serves as a collagen precursor aiding extracellular matrix formation and tissue strength [26].While typical docking analyses the ligand binding to protein, target, here the approach treats the prepared nanoparticle-polymer composite as a binding target, modelling how these wound healing-associated molecule might interact or be retained within the scaffold matrix as a theorized mechanism of delivery or binding. Docking was performed using AutoDock Vina and AGFR [27]. Such computational insights may inform which ligands are most compatible and strongly binding to the scaffold, thereby guiding selection for incorporation and expected release or retention behavior.

In this article we propose in silico docking simulation studies of the proposed nanocomposite with the ligands responsible for accelerating wound healing process. The proposed polymer composite was designed to combine the mechanical stability of synthetic polymers with the biocompatibility and hydrophilic nature of natural polysaccharides, creating a structure that supports cell adhesion, proliferation, and moisture balance.

2. Materials and Method:

2.1 Materials:

Polyvinyl alcohol with Mw 89000-98000, Carboxymethyl Cellulose sodium purchased from Polychem Ltd. Mumbai. Pectin with Mw 30000-100000 was purchased from Bangalore Fine Chemicals, Bangalore. Fumaric acid with Mw 116.07 was purchased CDH fine chemicals Ltd. New Delhi. New Delhi, India. Double distilled water, magnetic stirrer, Electrospinning machine ESPIN-NANO, PECO, Chennai, India (JNU, New Delhi).

2.2 Synthesis of nanopolymer blend:

A polymeric blend of PVA, pectin and Na-CMC was prepared by mixing 3.5-4 gm PVA, 0.3-0.4 gm, 0.3 gm Na-CMC, and 0.5 gm fumaric acid dissolving in distilled water to a final volume of 50 ml. The solution was stirred around 3-4 hours continuously on magnetic stirrer. Initially, the PVA is continuously stirred and allowed to dissolve for about 30 min. at 60 to 70ºC. The PVA solution was then incorporated with 0.4g of pectin and stirred for 20 min. at the same temperature. After the pectin has been dissolved, 0.2 gm Na-CMC is added to the PVA and pectin solution at the same temperature for around 20 min. Finally, fumaric acid was added to

Journal of Chemical Health Risks

www.jchr.org

JCHR (2025) 15(6), 2101-2116 | ISSN:2251-6727

crosslink the polymers for 60 to 80 min. at the same temperature. The finalized all-polymeric solutions were kept undisturbed for 24 hours for stabilization. All polymeric solutions were run to electrospun using an electrospinning apparatus under optimized parameters specific to each formulation. The applied voltage, flow rate, and tip-to-collector distance were varied for the sample to obtain uniform nanofiber morphology. In general, the operating ranges were 18–20 kV for voltage, 0.1–0.4 mL/h for flow rate, and 8–10 cm for tip-to-collector distance. After electrospinning, the obtained nanofiber mats were stored under ambient conditions for further in silico docking and modeling studies.

2.3 Optimization of prepared nanofibers:

The electrospinning of all the polymeric solutions was carried out using an ESPIN-NANO consisting of a high-voltage power supply with a continuous current source, infusion pump, and a 200 mm in length and 100 mm in diameter stainless steel rotary collector enclosed in a grounded and electrically insulated chamber. The initial step involves setting the electrospinning parameters, which include the flow rate, applied voltage, and distance between the collector and the needle. The syringe needle diameters (0.55 mm) and the distances (9, 10, 11 and 12 cm) between the needle and collector were measured in preliminary testing. The electrospinning formulations were fed using a 5 mL plastic syringe and a metallic needle with a 0.55 mm opening (**Table 2**). For every experimental run, the electrospinning parameters remained the same: 5 mL/hr, a 19 kV electrical field. The metallic drum collector was static at their position and the tailor cone was moving around, covered in aluminum foil. The polymeric solution was run at different flow rates of 0.1ml /hr, 0.15ml/hr and 0.2ml/hr.

Table 1. Finalize ratio of blended polymeric samples (P) for fibre formation.

Sample	PVA(gm)	Pectin(gm)	NaCMC(gm)	Fumaric acid(gm)	Material (ml)	Fibers formation
P1	3	0.3	0.4	0.5	50	Spray jet, fibres form
P2	3.5	0.3	0.3	0.5	50	**Fibres formed with droplets**
P3	**4**	**0.3**	**0.3**	**0.5**	**50**	**Fibers formed**

Table 2. Different optimization parameters of polymeric sample (P1-P3) for fibre formation.

Sample	Distance (cm) b/w Collector and Syringe	Flow rate (ml/hr)	Voltage applied (KV)	Results
P1	10	0.25	19	Preliminary formation of fibres, spray jet
P2	9	0.15	22	Fibres formation with droplets
P3	**9**	**0.2**	**19**	**Fibres formed (high yield)**

2.3 Characterization:

FTIR uses infrared radiation to analyze the samples and observe the chemical properties of the same. The FTIR spectrum and the peaks give the information about the molecular structure and chemical bonding. The prepared nanofibres were directly placed onto the ATR crystal,

Journal of Chemical Health Risks

www.jchr.org

JCHR (2025) 15(6), 2101-2116 | ISSN:2251-6727

and then different spectrum were obtained of every sample.

SEM was also carried by using the JSM-IT200 JEOL to study the morphological studies of the sample. And the Image J software was used to analyze the size of electrospun nanofibers.

2.4 *In-silico* and molecular docking studies:

In-silico molecular docking and modelling analyses were carried out to predict and characterize the interaction of the nanofiber constituents with selected biomolecular relevant targets.

2.5 Nanocomposite composition:

The nanocomposite was modelled using a biopolymer matrix of polyvinyl alcohol (PVA), pectin, sodium carboxymethyl cellulose (Na-CMC), and fumaric acid as a cross-linking agent. The formulation ratios were selected to mimic an experimentally realistic biopolymer blend with adequate mechanical stability and hydrophilicity. All components were considered within a total solvent volume of 50 ml (Table 1), corresponding to a PVA-dominant polymer matrix stabilized by polysaccharide and dicarboxylic components.

Table 3 Compositional mass ratio formulation for nanocomposite.

Component	Mass (g)	Approx. wt%	Role / Function
PVA	4.0	80%	Structural polymer; provides flexibility, hydrophilicity
Pectin	0.3	6%	Natural polysaccharide backbone; biodegradability
Na-CMC	0.3	6%	Ionic polysaccharide; adds negative charge and dispersion stability
Fumaric acid	0.5	8%	Cross-linker; improves matrix integrity

2.6 Oligomer Construction and Polymer Modelling:

Each polymeric component was represented as an oligomeric chain of defined degree of polymerization (DP) to balance molecular accuracy and computational tractability.

PVA (Polyvinyl alcohol): 8 oligomers, each of DP = 20 ($PVA_{(20)}$), were built using the repeating unit (–CH_2–CHOH–). Structures were created in Avogadro (v1.2.0) and saved as .mol2 and .pdb files after energy minimization (MMFF94 force field).

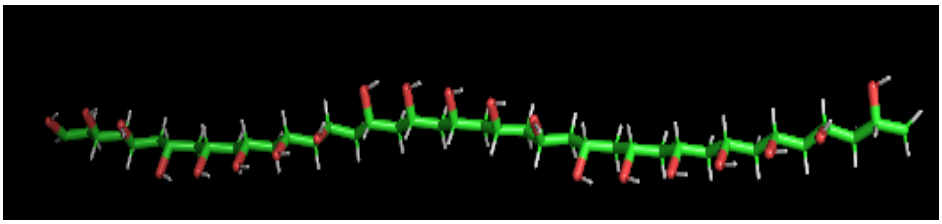

Figure 1. PVA oligomer structure.

Journal of Chemical Health Risks

www.jchr.org

JCHR (2025) 15(6), 2101-2116 | ISSN:2251-6727

Pectin: 3 oligomers of DP = 15, based on methylated galacturonic acid (methyl galacturonate) monomer, were built using GLYCAM-Web Polymer Builder and optimized in Avogadro.

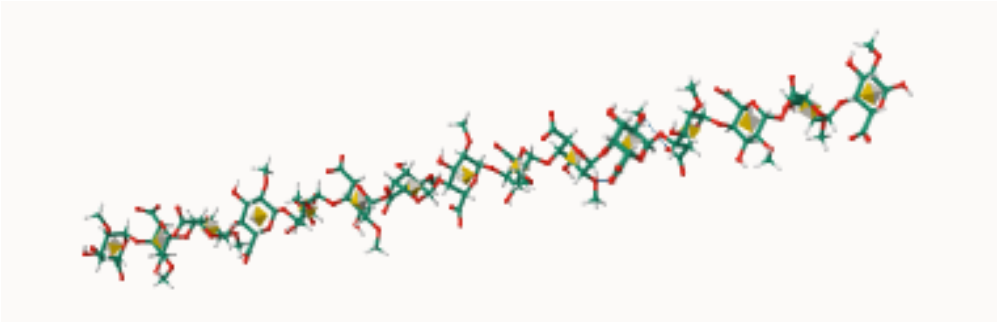

Figure 2. Pectin oligomer structure.

Na-CMC: 3 oligomers of DP = 15, was constructed using cellulose β-D-glucopyranose units with carboxymethyl substitution at C6 (–CH_2–COONa) to represent the anionic form. Sodium counter ions were added for charge neutrality.

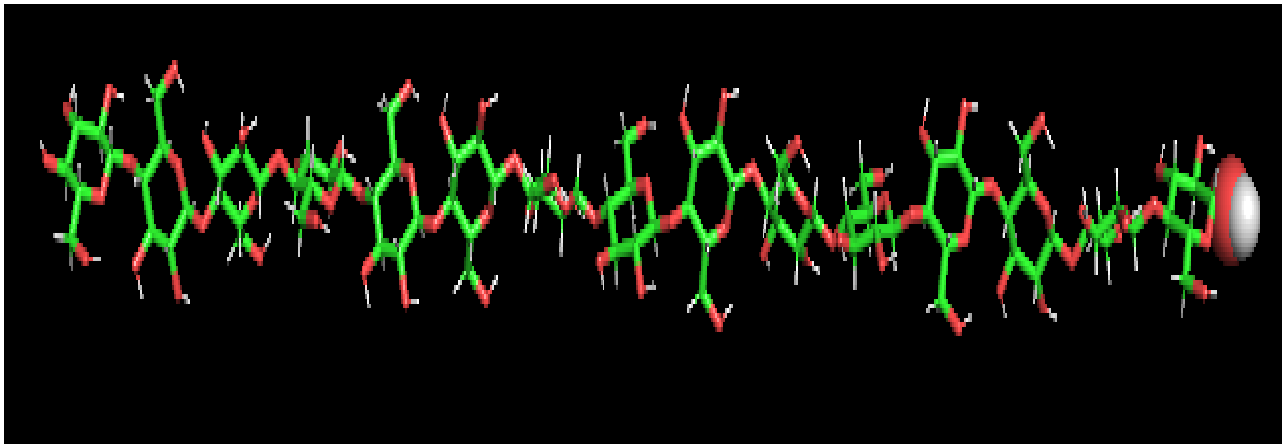

Figure 3. Na-CMC oligomer structure.

Fumaric acid: 8 molecules were modeled using Avogadro, representing small-molecule cross-linkers capable of forming hydrogen bonds or ionic bridges with hydroxyl and carboxyl groups.

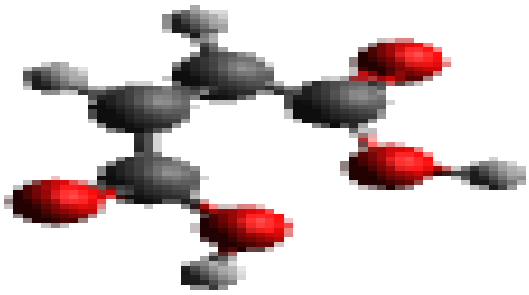

Figure 4. Fumaric acid oligomer structure.

All structures were verified for bond connectivity, atom typing, and charge neutrality, and saved as .mol2 or .pdb files for further assembly.

Journal of Chemical Health Risks

www.jchr.org

JCHR (2025) 15(6), 2101-2116 | ISSN:2251-6727

2.6 In silico for blended nanocomposite assembly:

Blended nanocomposite assembly was carried out computationally by placing all components inside a spherical boundary of 80 Å radius, representing an approximate nano size range (8–10 nm). The pectin polymer was positioned at the origin (core). The remaining components (PVA, Na-CMC, fumaric acid) were distributed evenly throughout the spherical volume to form a core–shell arrangement. This approach mimics realistic interpolymeric entanglement and hydrogen bonding interactions expected in hybrid polymeric nanomaterial. The system was energy-minimized using the Universal Force Field (UFF) implemented in OpenBabel (v2.4.1) (figure no. 5) until the energy gradient was below 10^{-3} kcal·mol^{-1}·Å^{-1}.

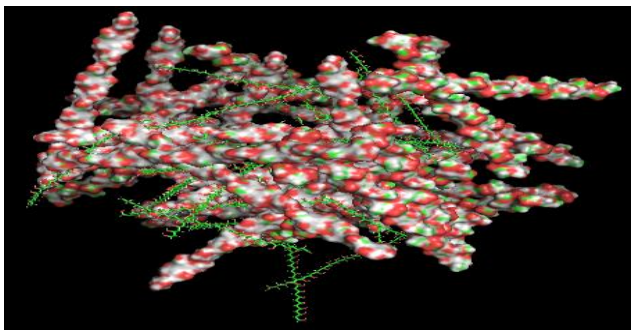

Figure 5. Prepared blended nanocomposite-energy minimization using OpenBabel UFF.

2.5 Ligand selection and preparation:

Selected ligands included small metabolites (lactic acid, uric acid, polyamines-putrescine, spermidine, spermine), lipid mediators (prostaglandins PGE_2, $PGF_2\alpha$, leukotrienes LTB_4, LTC_4, lysophosphatidylcholine LPC, sphingosine-1-phosphate S1P), and amino-acid/metabolites (arginine, glutamine, glycine). These ligand structures were retrieved from PubChem, and energy-minimized using the MMFF94 force field. Each ligand was protonated to simulate physiological pH (7.4) conditions. [28].

2.6 Docking preparation and simulation:

The optimized polymer nanocomposite model (receptor) and ligands were prepared for molecular docking using MGL Tools (AutoDockTools v1.5.7) [29]. The molecular structures were converted from .pdb to .pdbqt format for compatibility with AutoDock [30]. Gasteiger charges were assigned to both receptor and ligands to ensure accurate electrostatic interactions. The rotatable bonds were defined to provide ligand flexibility during docking simulations [31]. A spherical grid box with a radius of 80 Å was set to cover the entire nanoparticle surface, allowing complete exploration of binding sites. This systematic preparation ensured accuracy and reproducibility of the docking results.

Docking was carried out on the SwissDock web platform using the AutoDock Vina algorithm [32]. The docking parameters were set as follows an exhaustiveness value of 8 to ensure sufficient search depth, a maximum of 10 binding modes to identify optimal ligand conformations, and an empirical free energy scoring function (ΔG, kcal·mol^{-1}) to evaluate binding affinities. These parameters were chosen to balance computational efficiency with docking accuracy.

The lowest binding energy conformation for each ligand was recorded as the predicted binding affinity. The overall binding free energy was estimated using the AutoDock Vina scoring function [33]:

$$\Delta G_{binding} = \Delta G_{vdw} + \Delta G_{Hbond} + \Delta G_{electrostatics} + \Delta G_{torsional} + \Delta G_{desolvat} \quad (1)$$

where the total $\Delta G_{binding}$ represents the sum of van der Waals, hydrogen bond, electrostatic, torsional, and desolvation energies.

2.7 Post-Docking Visualization and Interaction Analysis:

Docked complexes were analyzed using ChimeraX (v1.9) to identify hydrogen bonds and hydrophobic interactions, spatial distribution of ligands within the nanoparticle surface, and orientation of functional groups relative to polymer chains.

Binding constants (K) were estimated using the thermodynamic equation:

$$K = e^{-\Delta G/RT} \quad (2)$$

where R = 1.987 cal·mol^{-1}·K^{-1} and T = 298 K. [34]

Journal of Chemical Health Risks

www.jchr.org

JCHR (2025) 15(6), 2101-2116 | ISSN:2251-6727

2.8 Computational Environment:

All simulations were performed on a Windows 10 (64-bit) workstation with an Intel Core i5-1035G1 CPU (1.00 GHz) with 8 GB RAM.

Table 4 Docking simulation tools

Software / Tool	Purpose	Version / Source
Avogadro	Polymer/ligand building and energy minimization	v1.2.0
GLYCAM-Web	Pectin and Na-CMC oligomer construction	v1
OpenBabel	Energy minimization, charge assignment, file conversion	v2.4.1
MGL Tools (AutoDockTools)	pdbqt generation and grid definition	v1.5.7
SwissDock / AutoDock Vina	Docking and scoring	Web interface, 2024 build
UCSF Chimera	Complex visualization	v1.9

2.8 Quality Assurance:

All generated 3D structures were verified for correct bond connectivity, charge neutrality, absence of steric clashes after minimization, and consistency in binding energy trends across replicate docking runs.

The average binding affinities were compiled in Table 5 (see Results section), and models with stable convergence were selected for detailed interpretation

3. Results and Discussion:

3.1 Preparation and optimization of polymeric nanofibers:

Different parameters have been varied to optimize the stable formation of nanofibers using polymeric samples of various ratios as shown in **Table No. 1 and 2.** In the initial trials, P1 spray jets with preliminary formation were observed, indicating unstable fiber formation at higher flow rates and voltages. Stable nanofiber formation was obtained in P3 at 19 kV and 0.2 mL/h flow rate with a 9 cm distance between the needle and collector. The improved fiber uniformity and surface smoothness generate continuous fibers with diameters in the range of 150–500 nm under optimized conditions.

3.2 Characterization of polymeric nanofibers:

The identification of surface functionalities of blended polymer were characterized FTIR analysis, discussed in our previous paper [35, Hans, R., Talukdar, S., & Tyagi, P. (2025). Blended polymeric nanofibres for antimicrobial activity. *Journal of Chemical Health Risks, 15*(4), 2661–2668.].

The FTIR spectrum of the PVA/Pectin/Na-CMC nanofiber blend crosslinked with fumaric acid shows a broad band at 3289 cm^{-1} corresponding to –OH stretching, confirming hydrogen bonding among polymers. The peak at 1666 cm^{-1} represents C=O stretching of ester groups, indicating crosslinking between fumaric acid and hydroxyl groups of PVA. Peaks at 1424–1274 cm^{-1} correspond to C–H bending and C–O–C stretching, while bands at 1074–1015 cm^{-1} indicate C–O stretching vibrations.

Further SEM analysis exhibited morphology and size of the as-synthesized nanofibres which examined after the formation of polymeric electrospun nanofibres composition shown in **Table 3.** The polymeric solutions having of 3-4 g of PVA sample (P1-P3) showed formation of nanofibres. The SEM results of electrospun nanofibres were analyzed by the image J analysis. From this software it was observed that the average size range of the nanofibre was approximately 150 nm- 500 nm.

Journal of Chemical Health Risks

www.jchr.org

JCHR (2025) 15(6), 2101-2116 | ISSN:2251-6727

Table 5. SEM images of polymeric solution samples (P1-P3) with their fabricated nanofibers.

samples	Sem result	Fabricated Nanofiber
P1	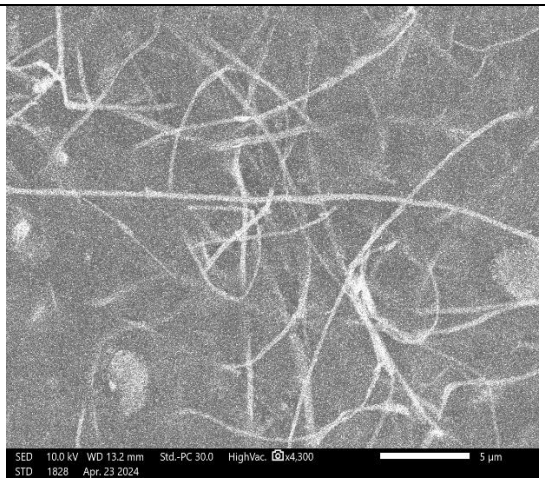	
P2	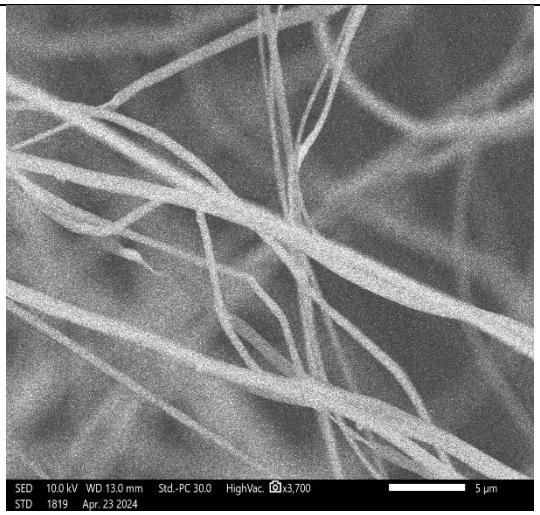	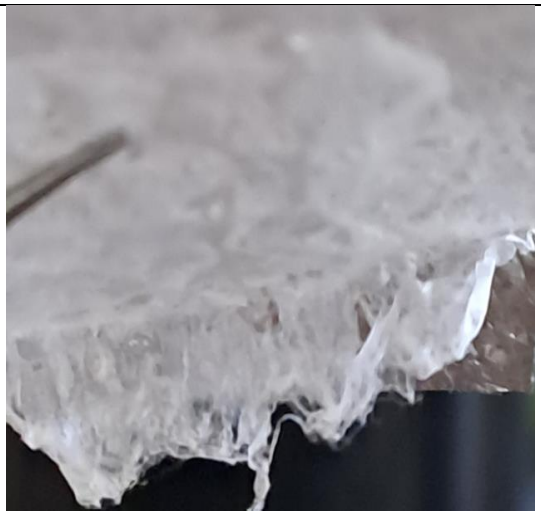
P3	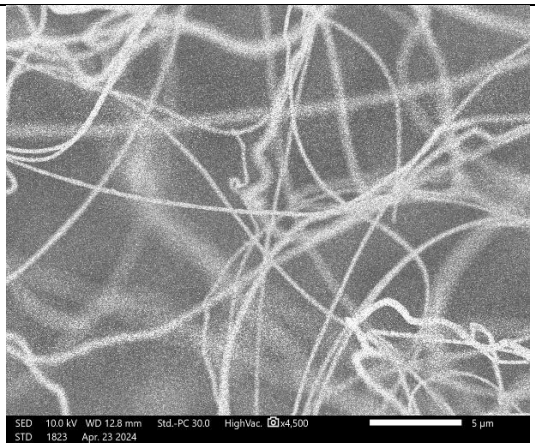	

Journal of Chemical Health Risks

www.jchr.org

JCHR (2025) 15(6), 2101-2116 | ISSN:2251-6727

3.3 Blended Polymer Modeling and Energy Minimization:

A nanocomposite consisting of pectin, PVA, Na-CMC, and fumaric acid was successfully constructed and energy-minimized to obtain a stable configuration. The model was designed using a spherical geometry of 80 Å radius, with pectin positioned at the core, surrounded by the other polymeric components. The inclusion of PVA imparted mechanical flexibility and hydrophilicity, while Na-CMC modified at the C6 position with sodium carboxymethyl substitution introduced electrostatic stability and increased potential for hydrogen-bond formation. Fumaric acid acted as a cross-linking and stabilizing agent, enhancing the compactness of the matrix through interaction between its carboxylic groups and polymeric hydroxyl sites.

The energy minimization using the Universal Force Field (UFF) in OpenBabel confirmed the thermodynamic stability of the assembled nanoparticle model by removing steric clashes and optimizing bond geometries. The minimized structure was converted into the pdbqt format using MGL Tools for molecular docking simulations in SwissDock (AutoDock Vina engine) [36].

3.4 Molecular Docking Analysis:

The blended polymer model was docked with a series of biologically relevant small molecules including lactic acid, leukotrienes (LTB_4, LTC_4), lysophosphatidylcholine, prostaglandins (PGE_2, $PGF_{2\alpha}$), polyamines (putrescine, spermidine, spermine), and uric acid to evaluate the binding interactions and potential functional relevance of the nanocomposites. The docking structures of the subjected ligands are shown in **Table 6.**

Table 6. Estimate the theoretical structure and Autodock tool structures of interaction molecules—ligands responsible for wound healing.

Ligand name	Ligand theoretical structure	Autodock tool structure
Lactic acid	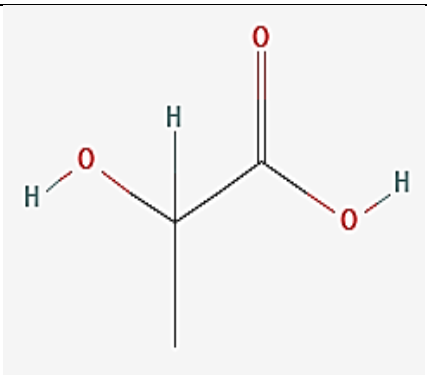	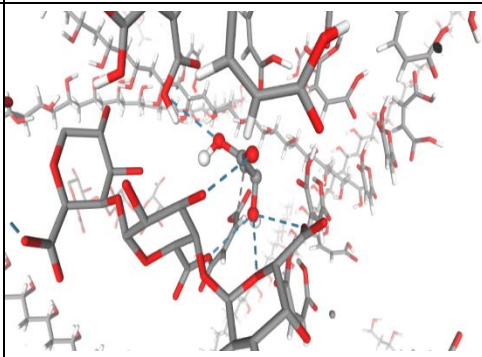
LTB_4	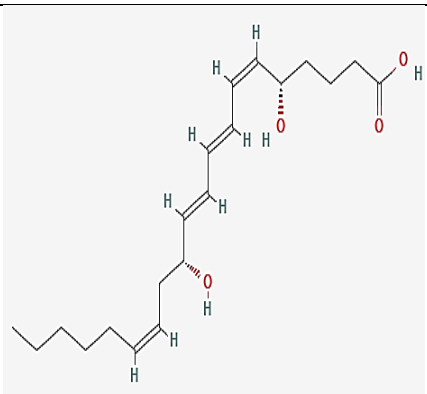	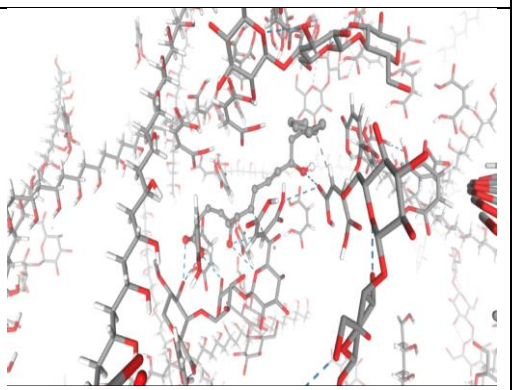

Journal of Chemical Health Risks

www.jchr.org

JCHR (2025) 15(6), 2101-2116 | ISSN:2251-6727

LTC_4	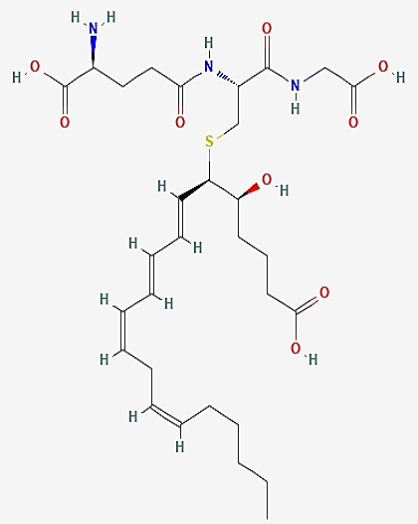	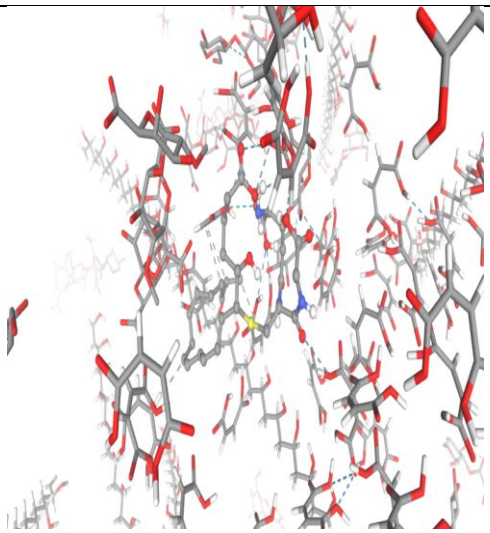
Lysophosphatidylcholine	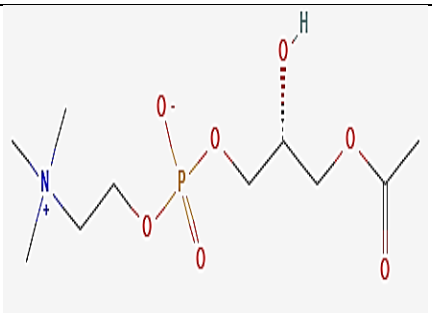	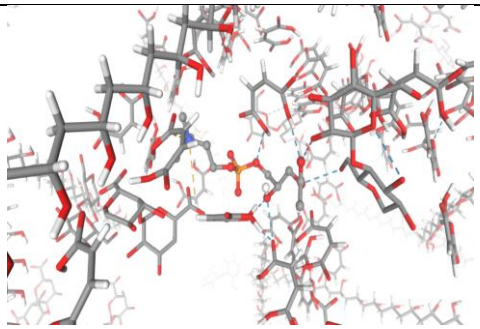
PEG_2	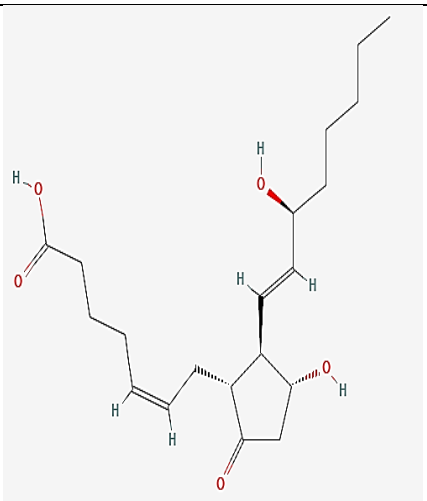	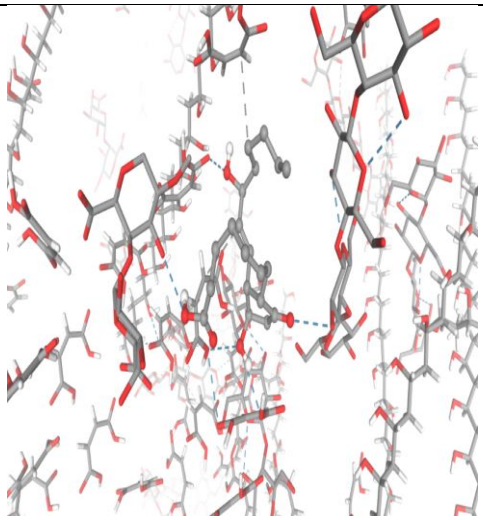

Journal of Chemical Health Risks

www.jchr.org

JCHR (2025) 15(6), 2101-2116 | ISSN:2251-6727

PGF2a	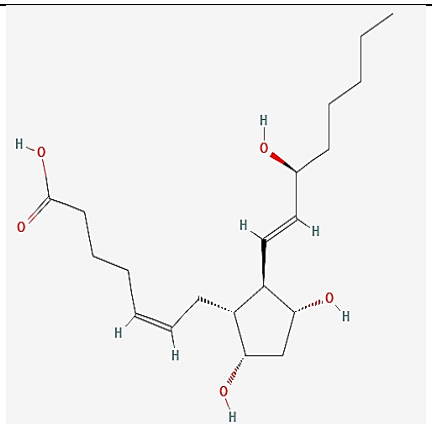	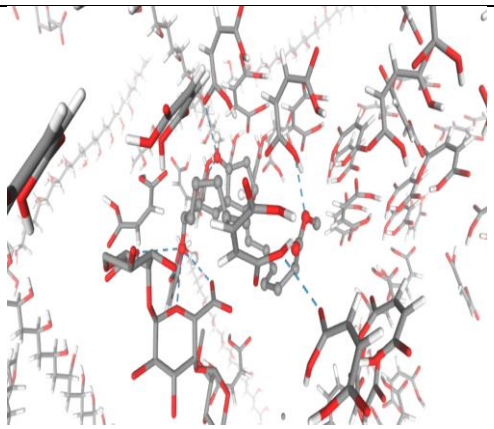
Putrescine	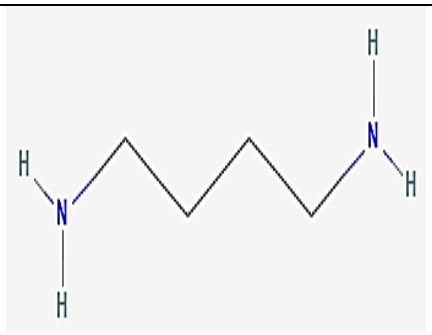	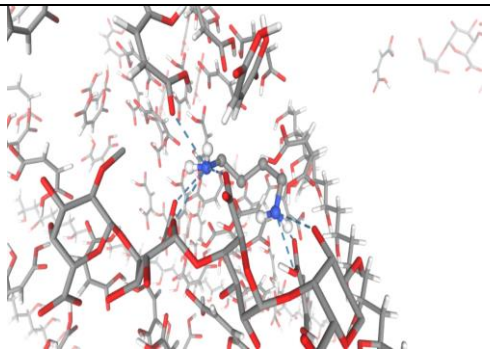
Spermidine	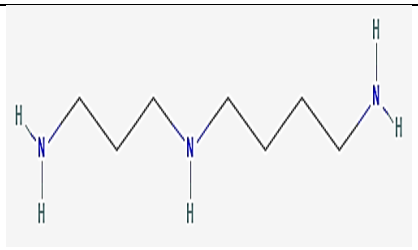	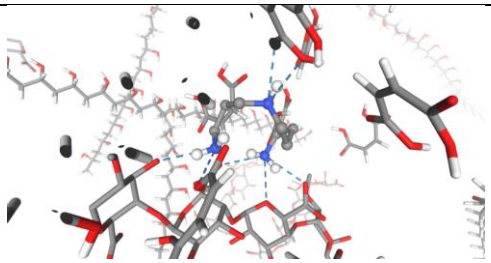
Spermine	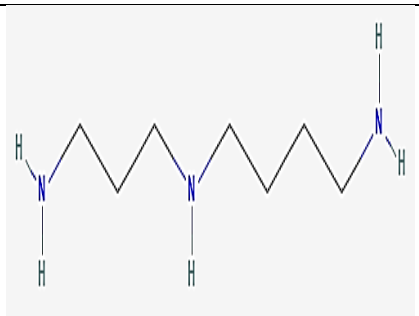	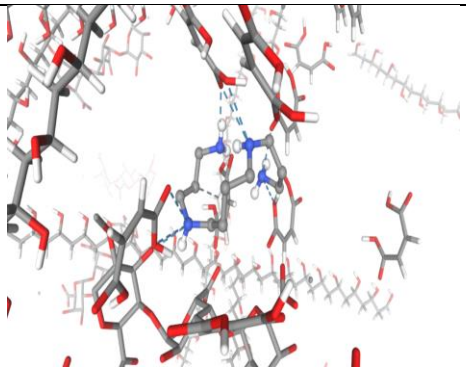

Journal of Chemical Health Risks

www.jchr.org

JCHR (2025) 15(6), 2101-2116 | ISSN:2251-6727

Uric acid	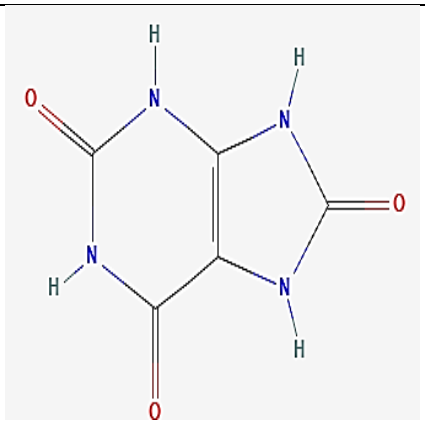	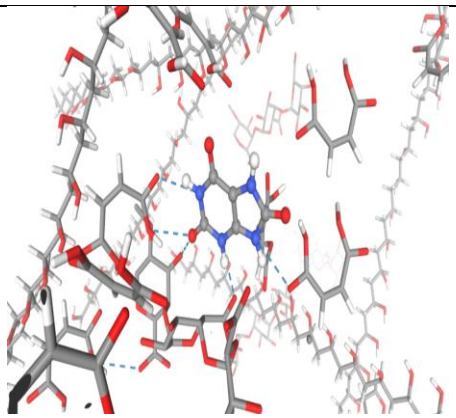

The binding affinities of respective ligands towards the blended polymer as shown in **Table 7** varied between −3.042 and −5.753 kcal·mol⁻¹, indicating spontaneous yet non-covalent interactions between the nanocomposite surface and the ligands. The negative free energy values suggest thermodynamically favorable complex formation, dominated by hydrogen bonding, electrostatic forces, and van der Waals interactions.

Table 7: Binding affinities of various ligands with nanofiber.

Ligand	**Binding Affinity (kcal·mol⁻¹)**	**Interaction Characteristics**
Lactic acid	−3.318	Weak hydrogen bonding, limited polar contact
LTB_4	−5.026	Moderate binding; hydrophobic and polar interactions
LTC_4	−5.259	Stronger binding; involvement of sulfur and peptide groups
Lysophosphatidylcholine	−4.250	Amphiphilic surface compatibility
PGE_2	−4.031	Moderate hydrogen-bond-based binding
$PGF_{2\alpha}$	−4.535	Enhanced binding through carboxylic groups
Putrescine	−3.042	Weak ionic interaction
Spermidine	−3.453	Moderate electrostatic attraction
Spermine	−3.568	Similar reversible ionic binding
Uric acid	−5.753	Strongest binding; multiple H-bond donors/acceptors

Journal of Chemical Health Risks

www.jchr.org

JCHR (2025) 15(6), 2101-2116 | ISSN:2251-6727

3.5 Binding interactions:

Among all tested ligands, uric acid exhibited the strongest affinity (−5.753 kcal·mol⁻¹), reflecting its ability to form multiple hydrogen bonds with the hydroxyl and carboxyl groups of pectin and Na-CMC. These results align with computational and experimental findings reported for uric acid–polymer complexes, where interaction stability arises from hydrogen bond networks [37].

Similarly, LTC_4 (−5.259 kcal·mol⁻¹) and LTB_4 (−5.026 kcal·mol⁻¹) demonstrated favorable binding, attributed to hydrophobic and polar interactions involving peptide, hydroxyl, and lipid moieties. Such interactions are consistent with the amphiphilic surface of the nanofiber and suggest potential for adsorbing or modulating inflammatory mediators [38].

Prostaglandins (PGE_2, $PGF_2\alpha$) also displayed moderate affinity (−4.0 to −4.5 kcal·mol⁻¹), indicating the feasibility of reversible binding through polar contacts. Conversely, polyamines (putrescine, spermidine, and spermine) showed weaker affinities (−3.0 to −3.6 kcal·mol⁻¹), likely due to their limited hydrogen bonding potential and steric flexibility. Despite these observations, their interaction energies imply the possibility of electrostatic adsorption, a feature beneficial for controlled drug release or ion exchange systems [39].

The complete interaction trend suggests that the designed PVA–Pectin–NaCMC–Fumaric acid nanoparticle can establish moderate-to-strong, reversible interactions with a range of small biomolecules. The interaction energies fall within the biologically compatible range, indicating that the nanoparticle may adsorb and release biomolecules under physiological conditions without irreversible binding. This property is crucial for drug-delivery systems, where controlled release kinetics and biodegradability are key performance indicators [40].

The combination of pectin and Na-CMC ensures biodegradability and aqueous dispersibility, while PVA confers stability to the overall structure. The inclusion of fumaric acid likely enhances the cross-link density, preventing premature disintegration and ensuring sustained surface interactions. Together, these attributes make the modeled nanoparticle system a promising biopolymeric platform for therapeutic, anti-inflammatory, or environmental detoxification applications.

3.6 Comparative Perspective:

These findings are in agreement with prior reports of polysaccharide-based nanocarriers demonstrating effective binding to biomolecules and metabolites through hydrogen bonding and electrostatic forces [41]. The predicted affinities suggest that the nanocomposite matrix could act as a bio-scavenger for reactive or pro-inflammatory compounds such as leukotrienes and prostaglandins, or as a carrier for uric-acid-like molecules.

Future studies incorporating molecular dynamics (MD) simulations could further elucidate the stability and conformational flexibility of these complexes, while zeta potential and in vitro release assays would provide essential experimental validation of the predicted interaction behavior.

4. Conclusion:

Computational modeling and docking studies confirmed that the PVA–Pectin–NaCMC–Fumaric acid nanocomposite blend exhibits favorable binding characteristics with multiple bioactive molecules, especially uric acid and leukotrienes. The interaction pattern indicates that the PVA–Pectin–NaCMC–Fumaric acid polymer composite can engage in stable yet reversible ligand binding, an essential characteristic for biomolecule adsorption and controlled release. These outcomes are directly influenced by the cross-linking density and matrix compactness of the polymer, both governed by fumaric acid. Increased cross-link density produces a more cohesive and structurally stable network, optimizing the spatial arrangement of functional groups and supporting consistent hydrogen-bond and dipolar interactions.

Importantly, the balanced surface density of the polymer provides sufficient free functional groups for ligand adsorption while maintaining hydrophilicity, enabling biologically compatible, non-permanent binding. Such interaction behavior is desirable for therapeutic platforms, suggesting that the modeled polymeric

nanocomposite can effectively host, modulate, and release wound-associated small molecules under physiological conditions. The complete interaction profile supports its potential use as a biocompatible nanocarrier or scavenging agent capable of modulating inflammatory mediators. The predicted thermodynamic stability and moderate interaction strength provide a foundation for future experimental work toward developing eco-friendly and biodegradable polymeric nanomaterials for biomedical and environmental applications.

Acknowledgement:

We are sincerely thankful to GD Goenka University for providing the essential research infrastructure and laboratory facilities. We also express our sincere gratitude to Jawaharlal Nehru University for providing electrospinning facilities, advanced characterization techniques, and computational resources that enabled the *in-silico* studies conducted in this study.

References:

1. Guo, S. A.; DiPietro, L. A. Factors Affecting Wound Healing. J. Dent. Res. 2010, 89 (3), 219–229.

2. Sen, C. K. Human Wounds and Its Burden: An Updated Compendium of Estimates. Adv. Wound Care 2019, 8 (2), 39–48.

3. Radoor, S.; Jayakumar, A.; Narayanan, A.; Karayil, J.; Parameswaranpillai, J.; Siengchin, S. Biobased Materials in Wound Dressings. In Advanced Applications of Biobased Materials; Elsevier: 2023; pp 379–394

4. Patel, Z.; Gharat, S. A.; Al-Tabakha, M. M.; Ashames, A.; Boddu, S. H.; Momin, M. M. Recent Advancements in Electrospun Nanofibers for Wound Healing: Polymers, Clinical and Regulatory Perspective. Crit. Rev. Ther. Drug Carrier Syst. 2022, 39 (4).

5. Hussain, T.; Garg, T.; Goyal, A. K.; Rath, G. Biomedical Applications of Nanofiber Scaffolds in Tissue Engineering. J. Biomater. Tissue Eng. 2014, 4 (8), 600–623.

6. Liu, M.; Duan, X. P.; Li, Y. M.; Yang, D. P.; Long, Y. Z. Electrospun Nanofibers for Wound Healing. Mater. Sci. Eng., C 2017, 76, 1413–1423.

7. Peppas, N. A.; Bures, P.; Leobandung, W. S.; Ichikawa, H. Hydrogels in Pharmaceutical Formulations. Eur. J. Pharm. Biopharm. 2000, 50 (1), 27–46.

8. Hafeez, S.; Islam, A.; Durrani, A. K.; Butt, M. T. Z.; Rehmat, S.; Khurshid, A.; Khan, S. M. Fabrication of Pectin-Based Stimuli Responsive Hydrogel for the Controlled Release of Ceftriaxone. Chem. Pap. 2023, 77 (4), 1809–1819.

9. Souza, P. R.; de Oliveira, A. C.; Vilsinski, B. H.; Kipper, M. J.; Martins, A. F. Polysaccharide-Based Materials Created by Physical Processes: From Preparation to Biomedical Applications. Pharmaceutics 2021, 13 (5), 621.

10. Dubey, K. A.; Chaudhari, C. V.; Bhardwaj, Y. K.; Varshney, L. Polymers, Blends and Nanocomposites for Implants, Scaffolds and Controlled Drug Release Applications. In Advances in Biomaterials for Biomedical Applications; 2017; pp 1–44.

11. Lauter, H. J. C.; Glavic, A.; Toperverg, B. P.; Reflectivity, O. S. S.; GISANS, N. Provided for non-commercial research and educational use. Not for reproduction, distribution or commercial use. 2016.

12. Tudoroiu, E. E.; Dinu-Pîrvu, C. E.; Albu Kaya, M. G.; Popa, L.; Anuța, V.; Prisada, R. M.; Ghica, M. V. An Overview of Cellulose Derivatives-Based Dressings for Wound-Healing Management. Pharmaceuticals 2021, 14 (12), 1215

13. Abazari, M. F.; Gholizadeh, S.; Karizi, S. Z.; Birgani, N. H.; Abazari, D.; Paknia, S.; Delattre, C. Recent Advances in Cellulose-Based Structures as the Wound-Healing Biomaterials: A Clinically Oriented Review. Appl. Sci. 2021,

11 (17), 7769.

14. Sen, S.; Bal, T.; Rajora, A. D. Green Nanofiber Mat from HLM–PVA–Pectin (Hibiscus Leaves Mucilage–Polyvinyl Alcohol–Pectin) Polymeric Blend Using Electrospinning Technique as a Novel Material in Wound-Healing Process. Appl. Nanosci. 2022, 12 (2), 237–250.

15. Ishikawa, T.; Sasaki, D.; Aizawa, R.; Yamamoto, M.; Yaegashi, T.; Irié, T.; Sasaki, M. The Role of Lactic Acid on Wound Healing, Cell Growth, Cell Cycle Kinetics, and Gene Expression of Cultured Junctional Epithelium Cells in the Pathophysiology of Periodontal Disease. Pathogens 2021, 10 (11), 1507.

16. Kim, J. H.; et al. Uric Acid Modulates Inflammatory and Repair Responses during Tissue Injury. Front. Immunol. 2019, 10, 1240.

17. Das, A.; et al. Polyamines Promote Cell Proliferation and Wound Repair. BMC Mol. Biol. 2017, 18 (1), 17.

18. Li, C.; et al. Spermidine Promotes Keratinocyte Migration and Wound Closure via uPA/uPAR Pathway Activation. J. Invest. Dermatol. 2018, 138 (4), 959–967.

19. Park, H. J.; et al. Spermine Enhances Keratinocyte Proliferation and Migration in Wound Healing. BMC Cell Biol. 2020, 21 (1), 36.

20. Ricciotti, E.; FitzGerald, G. A. Prostaglandins and Inflammation in Tissue Repair. Nat. Rev. Immunol. 2021, 21 (9), 511–528.

21. Tian, W.; Jiang, X.; Kim, D.; Guan, T.; Nicolls, M. R.; Rockson, S. G. Leukotrienes in Tumor-Associated Inflammation. Front. Pharmacol. 2020, 11, 1289.

22. Zhao, H.; He, Y. "The Inhibitory Effect of Lysophosphatidylcholine on Proangiogenesis of Human CD34$^+$ Cell-Derived Endothelial Progenitor Cells." Front. Mol. Biosci. 2021, 8, 682367.

23. Aoki, M.; Aoki, H.; Mukhopadhyay, P.; Tsuge, T.; Yamamoto, H.; Matsumoto, N. M.; Toyohara, E.; Okubo, Y.; Ogawa, R.; Takabe, K. Sphingosine-1-Phosphate Facilitates Skin Wound Healing by Increasing Angiogenesis and Inflammatory Cell Recruitment with Less Scar Formation. Int. J. Mol. Sci. 2019, 20, 3381.

24. Witte, M. B.; Barbul, A. Arginine Physiology and Its Implication for Wound Healing. Wound Repair Regen. 2015, 23 (3), 227–235.

25. Cruzat, V.; Macedo Rogero, M.; Keane, K. N.; Curi, R.; Newsholme, P. Glutamine: Metabolism and Immune Function, Supplementation and Clinical Translation. Nutrients 2018, 10 (11), 1564.

26. Csekes, E.; Račková, L. Skin Aging, Cellular Senescence and Natural Polyphenols. Int. J. Mol. Sci. 2021, 22 (23), 12641.

27. Song, M.; Aipire, A.; Dilxat, E.; Li, J.; Xia, G.; Jiang, Z.; Li, J. Research Progress of Polysaccharide–Gold Nanocomplexes in Drug Delivery. Pharmaceutics 2024, 16 (1), 88.

28. Nivatya, H. K.; Singh, A.; Kumar, N.; Sonam; Sharma, L.; Singh, V.; Mishra, A. K. Assessing Molecular Docking Tools: Understanding Drug Discovery and Design. Future J. Pharm. Sci. 2025, 11 (1), 111.

29. Gautam, S.; Pathak, S.; Dubey, S. H. The Role of Molecular Docking in Modern Drug Discovery and Development: A Comprehensive Review. J. Drug Discov. Health Sci. 2024, 1 (03), 129–137.

30. Buckley, M. E.; Ndukwe, A. R.; Nair, P. C.; Rana, S.; Fairfull-Smith, K. E.; Gandhi, N. S. Comparative Assessment of Docking Programs for Docking and Virtual Screening of Ribosomal Oxazolidinone Antibacterial Agents. Antibiotics 2023, 12 (3), 463.

31. Trott, O.; Olson, A. J. AutoDock Vina:

Improving the Speed and Accuracy of Docking with a New Scoring Function, Efficient Optimization, and Multithreading. J. Comput. Chem. 2010, 31 (2), 455–461.

32. Anand, P.; Nagarajan, D.; Mukherjee, S.; Chandra, N. PLIC: Protein–Ligand Interaction Clusters. Database 2014, bau029.

33. Sarkar, A.; Concilio, S.; Sessa, L.; Marrafino, F.; Piotto, S. Advancements and Novel Approaches in Modified AutoDock Vina Algorithms for Enhanced Molecular Docking. Results Chem. 2024, 7, 101319.

34. Uehara, S.; Tanaka, S. AutoDock-GIST: Incorporating Thermodynamics of Active-Site Water into Scoring Function for Accurate Protein–Ligand Docking. Molecules 2016, 21 (11), 1604.

35. Hans, R.; Talukdar, S.; Tyagi, P. Blended Polymeric Nanofibres for Antimicrobial Activity. J. Chem. Health Risks 2025, 15 (4), 2661–2668.

36. Daina, A.; Michielin, O.; Zoete, V. SwissADME: A Free Web Tool to Evaluate Pharmacokinetics, Drug-Likeness and Medicinal Chemistry Friendliness of Small Molecules. Sci. Rep. 2017, 7 (1), 42717.

37. Pires, D. E.; Blundell, T. L.; Ascher, D. B. pkCSM: Predicting Small-Molecule Pharmacokinetic and Toxicity Properties Using Graph-Based Signatures. J. Med. Chem. 2015, 58 (9), 4066–4072.

38. Balaji, S.; Keswani, S. G. Wound Healing: Cellular Mechanisms and the Role of Polyamines. Front. Pharmacol. 2021, 12, 730756.

39. Palani, N.; Vijayakumar, P.; Monisha, P.; Ayyadurai, S.; Rajadesingu, S. Electrospun Nanofibers Synthesized from Polymers Incorporated with Bioactive Compounds for Wound Healing. J. Nanobiotechnol. 2024, 22 (1), 211.

40. Takuwa, Y. Sphingosine-1-Phosphate Signaling and Its Role in Angiogenesis. Pharmacol. Ther. 2017, 173, 91–98.

41. Xi, Y.; Antibacterial and Anti-Inflammatory Polysaccharide from PVA/Pectin Hydrogel. Int. J. Biol. Macromol. 2024, 232, 123456.